



Endothelial-specific *Crifl* deletion induces BBB maturation and disruption via the alteration of actin dynamics by impaired mitochondrial respiration

Journal of Cerebral Blood Flow & Metabolism
2020, Vol. 40(7) 1546–1561
© The Author(s) 2020
Article reuse guidelines:
sagepub.com/journals-permissions
DOI: 10.1177/0271678X19900030
journals.sagepub.com/home/jcbfm



Min Joung Lee^{1,2,3,*}, Yunseon Jang^{1,2,3,*}, Jeongsu Han^{1,2} ,
Soo J Kim^{1,2,3}, Xianshu Ju^{1,3}, Yu Lim Lee^{1,3}, Jianchen Cui^{1,3},
Jiebo Zhu^{1,2,3}, Min Jeong Ryu², Song-Yi Choi⁴,
Woosuk Chung^{1,5,6}, Chaejeong Heo^{7,8}, Hyon-Seung Yi⁹,
Hyun Jin Kim⁹, Yang H Huh¹⁰, Sookja K Chung¹¹,
Minho Shong^{9,12}, Gi-Ryang Kweon^{1,2} and Jun Young Heo^{1,2,3} 

Abstract

Cerebral endothelial cells (ECs) require junctional proteins to maintain blood–brain barrier (BBB) integrity, restricting toxic substances and controlling peripheral immune cells with a higher concentration of mitochondria than ECs of peripheral capillaries. The mechanism underlying BBB disruption by defective mitochondrial oxidative phosphorylation (OxPhos) is unclear in a mitochondria-related gene-targeted animal model. To assess the role of EC mitochondrial OxPhos function in the maintenance of the BBB, we developed an EC-specific *CR6-interactin factor 1* (*Crifl*) deletion mouse. We clearly observed defects in motor behavior, uncompact myelin and leukocyte infiltration caused by BBB maturation and disruption in this mice. Furthermore, we investigated the alteration in the actin cytoskeleton, which interacts with junctional proteins to support BBB integrity. Loss of *Crifl* led to reorganization of the actin cytoskeleton and a decrease in tight junction-associated protein expression through an ATP production defect in vitro and in vivo. Based on these results, we suggest that mitochondrial OxPhos is important for the maturation and maintenance of BBB integrity by supplying ATP to cerebral ECs.

Keywords

Crifl, endothelial cells, mitochondrial OxPhos, ATP depletion, blood–brain barrier

Received 9 August 2019; Revised 15 December 2019; Accepted 16 December 2019

¹Department of Medical Science, Chungnam National University, Daejeon, Republic of Korea

²Department of Biochemistry, Chungnam National University, Daejeon, Republic of Korea

³Infection Control Convergence Research Center, College of Medicine, Chungnam National University, Daejeon, Republic of Korea

⁴Department of Pathology, Chungnam National University, Daejeon, Republic of Korea

⁵Department of Anesthesiology and Pain Medicine, School of Medicine, Chungnam National University, Daejeon, Republic of Korea

⁶Department of Anesthesiology and Pain medicine, Chungnam National University Hospital, Daejeon, Republic of Korea

⁷Center for Integrated Nanostructure Physics (CINAP), Institute for Basic Science (IBS), Suwon, South Korea

⁸Center for Neuroscience Imaging Research (CNIR), Institute for Basic Science (IBS), Suwon, South Korea

⁹Department of Internal Medicine, Chungnam National University Hospital, Daejeon, Republic of Korea

¹⁰Electron Microscopy Research Center, Korea Basic Science Institute, Cheongju, Chungcheongbukdo, Republic of Korea

¹¹Medical Faculty at Macau University of Science and Technology, Taipa, Macau

¹²Research Center for Endocrine and Metabolic Diseases, Chungnam National University School of Medicine, Daejeon, Republic of Korea

*Min Joung Lee and Yunseon Jang contributed equally to this work.

Corresponding authors:

Jun Young Heo and Gi-Ryang Kweon, Department of Medical Science, Chungnam National University School of Medicine, Munhwa-Dong, Jungu, Daejeon 35015, Republic of Korea.

Emails: junyoung3@gmail.com; mitochondria@cnu.ac.kr

Introduction

An insufficient supply of energy by mitochondria to cerebrovascular endothelial cells (ECs) exacerbates cerebrovascular and neurodegenerative diseases.¹ Pharmacological inhibition of mitochondria induces disruption of tight junction proteins that function in the blood–brain barrier (BBB) and aggravates stroke outcomes in an in vivo ischemic stroke model.² In addition, oxygen–glucose deprivation and reoxygenation induce breakdown of tight junctions through increases in reactive oxygen species formation and changes in cytochrome c levels in ECs.³ MiR-34a disturbs BBB maintenance by reducing mitochondrial OxPhos and cytochrome c levels in cerebrovascular ECs.⁴ Although inhibition of mitochondrial respiration has been considered detrimental to BBB maintenance, the underlying mechanism of BBB disruption by mitochondrial dysfunction in ECs that specifically correlated with intracellular energy changes is poorly understood.

Cerebral ECs have approximately five times more mitochondria than ECs of peripheral capillaries, reflecting the higher demand for intracellular adenosine triphosphate (ATP) in the brain vasculature.^{5,6} In addition to its role in regulating the ATP-binding cassette (ABC) efflux transporter, P-glycoprotein, in the BBB, mitochondria-derived ATP regulates actin dynamics, providing the energy source that maintains proper organization of the actin cytoskeleton.⁷ The actin cytoskeleton, in turn, interacts with tight junction-associated proteins, including zonula occludens-1 (ZO-1) and occludin, which support tight junctions to preserve barrier function.^{8,9} Junction proteins function to form the selective permeability of the BBB and restrict the passage of toxic substances.¹⁰ By connecting ECs, these tight junction-associated proteins are indispensable for the maintenance of BBB integrity.¹¹ ATP depletion induces changes in G-actin (monomeric) and F-actin (filamentous) levels in ECs,¹² and dysregulation of actin dynamics disturbs tight junction assembly.¹³ Nevertheless, the relevance of mitochondrial respiration-derived ATP production capacity in the maintenance of intact structures of the BBB remains poorly understood.

ATP production by mitochondria is correlated with mitochondrial biogenesis and regulated by mitochondria-related genes such as *PGC1- α* (peroxisome proliferator-activated receptor gamma coactivator 1-alpha), *TFAM* (transcription factor A, mitochondrial) and NRF-1 (nuclear respiratory factors-1).¹⁴ *PGC1- α* upregulates mitochondrial biogenesis, indicated by the expression of mitochondrial antioxidant enzymes at the transcriptional level in normal ECs.¹⁵ *PGC1- α* activates TFAM, which induces mitochondrial biogenesis by modulating the expression of mtDNA genes¹⁶ and

upregulates NRF-1 to contribute to the expression of OxPhos subunits and mitochondrial transcription factors.¹⁷ Crif1 (CR6-interactin Factor1) is involved in the synthesis and insertion of OxPhos peptides in the inner membrane at the translational level, and the deletion of *Crif1* causes mitochondrial OxPhos dysfunction in mouse embryonic fibroblasts (MEFs).¹⁸ Downregulation of *Crif1* leads to disturbances in mitochondrial OxPhos complexes in peripheral ECs, and *Crif1* deficiency impairs vascular function.¹⁹ Although mitochondria in peripheral ECs have been investigated, there are few studies regarding mitochondria function in cerebral ECs, especially associated with mitochondrial OxPhos function and ECs in the BBB.⁶ We hypothesized that *Crif1* deletion in ECs leads to BBB maturation and disruption through mitochondrial dysfunction because ECs in the BBB have much more mitochondria than other ECs. We established an EC-specific *Crif1* deletion mouse (TEKCRIF1 mouse and endoxifen-induced VECad Cre-ER^{T2} transgenic mice). We demonstrated the relationship between mitochondrial function and BBB integrity and directly showed the pivotal contribution of mitochondria in the BBB, providing a new target for the regulation of BBB permeability in TEKCRIF1 mice and endoxifen-induced VECad Cre-ER^{T2} transgenic mice.

Materials and methods

Animals

We generated endothelial specific CRIF1 knockout mouse using TEK-Cre and VECad-CreER^{T2} mouse. TEK-Cre transgenic mice (C57BL/6J) were obtained from Jackson Laboratory (Bar Harbor, ME, USA). VECad (VE-cadherin) Cre-ER^{T2} transgenic mice²⁰ were transferred to and bred in our animal facility. Floxed *Crif1* mice were generated in a previous study.¹⁸ TEK-Cre transgenic mice (C57BL/6J) and floxed *Crif1* mice were crossed to generate TEKCRIF1 mice. Postnatal 11-day-old mice were used for experiments. VECad (VE-cadherin) Cre-ER^{T2} transgenic mice (C57BL/6J) and floxed *Crif1* mice were crossed to generate VECad Cre-ER^{T2}-*Crif1*^{flox/flox} mice. Six-week-old mice were used for experiments. We used TEK-Cre, *Crif1*^{+/+} for control, mentioned as WT. Mice were maintained in a controlled facility (temperature, 22–24°C; 12-h light/dark cycle). Animal experiments were approved by the Institutional Animal Care and Use Committee of Chungnam National University (ethical approval number, CNU-00912), and were in accordance with the ARRIVE guidelines for reporting in vivo experiments and the guidelines of Chungnam National University, School of Medicine.

Genomic PCR

Mice were genotyped by PCR with a *Cre* primer (F: 5'-GCGGTCTGGCAGTAAAACTATC-3', R: 5'-GTGAAACAGCATTGCTGTCACTT-3') and *Crif1* primer (F: 5'-GGGCTGGTGAAATGTGTTG-3', R: 5'-TCAGCTAGGGTGGGACAGA-3') with the following PCR conditions: 95°C for 5 min; 30 cycles of 95°C for 30 sec, 67°C for 30 s, and 72°C for 30 s; then 72°C for 5 min. Amplified DNA was analyzed using electrophoresis with a 3% agarose gel.

Cell culture and transfection

bEnd.3 [BEND3] cells (ATCC® CRL2299™) were purchased from ATCC (American Type Culture Collection, USA) and cultured in Dulbecco's modified Eagle's medium with 5% fetal bovine serum and 1% penicillin streptomycin at 37°C and 5% CO₂. bEnd.3 cells were transfected with siRNA for *Crif1* (siRNA sequence: 5'-GGAGUGCUCGCUUCCAGGAACU AUU-3') and negative control siRNA using Lipofectamine 3000 and RNAi max (Invitrogen, Carlsbad, CA, USA).

Immunohistochemistry

For CD45 staining, sections were deparaffinized, blocked in PBS containing 2% donkey serum (Gene Tex, CA, USA) and 0.3% Triton X-100 for 1.5 h, and then incubated with anti-CD45 antibody (Abcam, CA, USA). The sections were then washed with PBS and incubated with HRP-conjugated secondary antibody. After washing with PBS, the sections were slide-mounted and imaged using a microscope.

Immunocytochemistry

Coverslips were coated with poly-D-lysine and dry for 1 h at 37°C. Cells were seeded on the coverslips, and *Crif1* gene expression was knocked down for 48 h. The cells were washed with warm PBS and fixed with 4% paraformaldehyde for 20 min. After being washed with PBS, it was permeabilized with 0.1% TritonX-100 in 0.02% BSA-containing PBS for 30 min, blocked in 3% BSA with PBS for 30 min and incubated with a primary antibody for 1.5 h. After being washed with 0.2% BSA in PBS for three times, it was incubated with the secondary antibody for 2 h. After mounting, the samples were observed using a confocal microscope (Leica, Bensheim, Germany).

Immunofluorescence staining

TEKCRIF1 mice were perfused and fixed with 4% paraformaldehyde. Brain samples were dehydrated in 30% sucrose solution at 4°C. Then, the samples were

frozen and sliced into coronal sections to a thickness of 30 μm using a cryotome. The sections were stored in tissue stock solution and washed in PBS. The sections were blocked in 2% donkey serum (Gene Tex, CA, USA), 0.3% Triton X-100 with PBS for 1.5 h and then incubated with anti-CD31 (Millipore, CA, USA), anti-NDUFA9 (Abcam, CA, USA), anti-occludin (Invitrogen, CA, USA), anti-albumin (Abcam, CA, USA), anti-Olig2 (R&D systems, MN, USA), anti-ZO-1 (Thermo Scientific, IL, USA), anti-MBP (Millipore), and Alexa-594 conjugated phalloidin (F-actin staining) antibodies overnight at 4°C. After being washed with PBS, it was incubated with the secondary antibodies (Jackson, PA, USA) for 1.5 h at room temperature. After the tissue was mounted on slides using fluorescent mounting solution (Dako North America Inc., USA), the slides were imaged using an Olympus confocal microscope (Olympus, Lisbon, Portugal) and Leica confocal microscope (Leica, Bensheim, Germany).

In vivo dextran-FITC BBB permeability assay

TEKCRIF1 mice were anesthetized with 3.0% and 1.3% of isoflurane (VetEquip, Livermore, CA, USA) during surgery and two-photon imaging, respectively. The mouse head was fixed on a stage in a stereotaxic system with ear bars and the skull of the mice was exposed after removal of the scalp, and the skull was thinned by the drill to create an optical transcranial window. The head frame was attached onto the dried skull tightly with dental cement to secure the mouse head at the head holder in the imaging stage.²¹ To prevent skull dry-out during the image, we covered a PDMS film on the exposure skull. The mouse intracardially injected once by a syringe with dextran-FITC (40 kDa) before positioned on the imaging stage in the microscope. The mouse head was fixed on a stage by the head frame and the cerebral blood vessels represented by dextran-FITC were observed in the process of time using a TCS SP8 two-photon microscope (Leica, Mannheim, Germany) at 5 min approximately and at 30 min after one dextran injection. Two-photon imaging was conducted at a wavelength of 880 nm (3200 mW), delivered by a Chameleon Vision II two-photon laser (Coherent, Santa Clara, CA, USA).

Open-field test

Each mouse was placed in a 12 × 12 × 8-cm box. Movement was recorded for 10 min and analyzed with EthoVision XT 11.5 software.

Western blot analysis

Proteins were extracted from cortex and striatum with RIPA lysis buffer with phosphatase and protease inhibitor cocktail (Roche, Switzerland) and homogenized. Isolated protein by centrifuging at 16,000 r/min (each 20 μ g protein) was separated by electrophoresis using SDS-PAGE and then was transferred to PVDF membrane. The membranes were blocked with 5% BSA in TBST for 1 h at room temperature. Then, membranes were incubated at 4°C, overnight with anti-occludin antibody (Abcam, CA, USA), anti-actin antibody (Cytoskeleton, Inc, CO, USA) and washed three times for 10 min in TBS/T. After incubation with horseradish peroxidase-conjugated secondary antibody for 2 h at room temperature, membranes were washed three times for 15 min in TBS/T. Antibody-labeled proteins were detected by the ECL solution (WEST-ZOL).

Isolated mitochondrial oxygen consumption rate analysis in vivo

To analyze the OCR of mitochondria isolated from the cortex and striatum of the TEKCRIF1 mice, mitochondria were prepared from the cortex and striatum of the TEKCRIF1 mice using mitochondria isolation buffer (70 mM sucrose, 210 mM mannitol, 5 mM HEPES, 1 mM EGTA, 0.5% fatty acid-free BSA, pH 7.2) on ice. Isolated mitochondria were seeded at 25 μ g per well and diluted with mitochondria assay buffer (70 mM sucrose, 220 mM mannitol, 10 mM KH_2PO_4 , 5 mM MgCl_2 , 2 mM HEPES, 1 mM EGTA, 0.2% fatty acid-free BSA, 10 mM succinate, 2 μ M rotenone, pH 7.2), and 590 μ l assay media was added to each well. Ports of the XF 24 biosensor cartridge were injected with 40 mM ADP (final conc. 4 mM), 20 μ g/ml oligomycin (final conc. 2 μ g/ml), 50 μ M CCCP (final conc. 5 μ M) and 40 μ M antimycin A (cytochrome C reductase inhibitor, final conc. 4 μ M), and OCR analysis was performed at 37°C.

Transmission electron microscopy

Samples were extracted from the cortex and striatum. The samples were fixed with 2.5% glutaraldehyde-2% paraformaldehyde in 0.15 M sodium cacodylate buffer (pH 7.4) for 2 h at 4°C. After washed with sodium cacodylate buffer, the samples were fixed in 2% osmium tetroxide-1.5% ferrocyanide in 0.15 M cacodylate buffer (pH 7.4) for 1 h, incubated with 1% TCH for 30 min and treated with 2% OsO_4 for 30 min. For en bloc staining, the samples were incubated with 1% uranyl acetate overnight at 4°C, followed by incubation with lead citrate for 30 min at 60°C. The samples were dehydrated in an ethanol and propylene oxide series, embedded in an Epon 812 mixture and incubated with

pure resin at 70°C for 24 h for polymerization. The samples were sliced with an ultramicrotome (Ultra cut-UCT; Leica, Vienna, Austria) and then collected on 150-mesh copper grids. The ultrathin sections were observed using a Bio-HVEM system (JEM-1400Plus at 120 kV and JEM-1000BEF at 1000 kV; JEOL, JAPAN).

ATP analysis

bEnd.3 cells were grown to 60 mm and transfected. The cells were washed with PBS, and 20,000 cells/ml were prepared for ATP analysis. An ATP analysis kit (ATPlite 1step, PerkinElmer, USA) was used following the manufacturer's instructions.

Stereotaxic injection of endoxifen

To activate *Cre* recombinase, 2.5 mM endoxifen hydrochloride hydrate (Sigma E8284) in 20% DMSO/PBS or 20% DMSO/PBS, as a control, injected into the striatum of VECad *Cre-ER^{T2}-Crf1^{fllox/fllox}* mice (AP +0.7 mm, ML \pm 2.1 mm, DV $-$ 3.5 mm relative to the bregma; 0.2 μ l/min, total 2 μ l) using 33 G blunt needle and 10 μ l Hamilton syringe. The experiment was performed under anesthesia induced by sevoflurane. Mice will show symptoms such as weight loss and sickness if they were damaged during surgery. There were no defective mice in our experiments. Ten days after stereotaxic injection, the mice were analyzed.

Isolation of microvessels from brain tissue

Mice brain tissue without the cerebellum was transferred to MCDB 131 medium (Thermo Fisher, Gibco®, 10372019). The tissue was homogenized in 1 ml of MCDB 131 medium using 10 strokes of a tissue grinder. After adding 7 ml of MCDB 131 medium for balancing, the cells were centrifuged at 2000g for 5 min at 4°C. The supernatant was removed, and the pellet was resuspended in 8 ml of 15% dextran/PBS (Sigma-Aldrich, 31390). The samples were centrifuged at 10,000g for 15 min at 4°C. Then, the supernatants were removed carefully, and the pellets were washed using 1 ml of PBS. Next, the pellets were transferred to a 40- μ m cell strainer with 10 ml of PBS for washing. The filter was inverted, and the microvessels were collected using 10 ml of 0.5% BSA/MCDB 131 medium. The samples were centrifuged at 5000g for 10 min at 4°C, and the resulting pellets contained the microvessels.²²

Statistical analysis

All results are presented as the mean values \pm SD. The statistical significance of all the results was analyzed by

a two-tailed unpaired Student's *t* test using GraphPad Prism (GraphPad Software Inc., San Diego, CA, USA). The statistical significance of all the data is indicated by **P* < 0.05, ***P* < 0.01, or ****P* < 0.001.

Results

Crif1 deletion in ECs leads to abnormal behavioral activities in TEKCRIF1 mice

To assess the importance of mitochondrial function in ECs for BBB maintenance, we established an endothelial cell-specific *Crif1* deletion mouse (*Tek-Cre, Crif1^{fllox/flox}* mice). To inactivate *Crif1* in ECs, we crossed *Crif1*-floxed C57BL6/J mice with *Tek-Cre* mice expressing *Cre* recombinase under the control of an endothelial promoter, tyrosine kinase, that we called TEKCRIF1 (*Tek-Cre, Crif1^{fllox/flox} homozygous*) mice (Figure 1(a)). TEKCRIF1 mice were genotyped by PCR of the *Crif1* gene and *Cre* recombinase (Figure 1(b)). *Crif1* deletion did not cause a loss of body weight or systemic inflammation (Supplementary Figure 1(a) to (c)). To observe mitochondrial function in cerebral ECs of BBB, we focused on the striatum and cortical region, areas that are particularly vulnerable to BBB disruption.²³ To this end, we examined changes in the expression of occludin, which is involved in BBB integrity. We found no difference in the expression of occludin between postnatal day 5 WT and TEKCRIF1 mice (Supplementary Figure 1(d)), but found a marked difference at postnatal day 11, indicative of alterations in the BBB with distinguishable behavioral defects. *Crif1* mRNA and protein expression were decreased in the cortex and striatum of TEKCRIF1 mice (Supplementary Figure 1(e) to (g)). To specifically examine the changes in *Crif1* expression of ECs, we isolated microvessels from the brains of TEKCRIF1 mice and found that *Crif1* expressed was decreased by 60% of that in WT mice (Figure 1(c) and (d)).

The BBB is the key structure that prevents the entry of pathogens and controls immune cells from the blood into the CNS parenchyma.²⁴ Since BBB disruption causes neurological and behavioral defects in CNS disorders,²⁵ we measured the movement of mice in the open-field test to determine whether behavioral abnormalities appear in TEKCRIF1 mice (Figure 1(e)). The movement distance of TEKCRIF1 mice for 10 min was approximately halved compared to that of WT mice (Figure 1(f)). Whereas WT mice moved throughout the open field, the TEKCRIF1 mice did not move easily, remaining in a limited portion of the field and collapsing due to weak limbs. To determine the relevance of these behavioral abnormalities to neurological functions, we compared the clinical score of the

behavioral deficits in TEKCRIF1 and WT mice according to the description in Table 4 (Figure 1(g)). Approximately 24% of TEKCRIF1 mice showed a limp tail, and nearly 41% of TEKCRIF1 mice were unable to move because of abnormalities in the hindlimbs or both hindlimbs and forelimbs. The increase in the clinical score in TEKCRIF1 mice was associated with brain tissue damage (Table 1).

Myelin is uncompacted, and leukocytes infiltrate the tissue of TEKCRIF1 mice

To determine the relevance of neurological pathologies for observed behavioral abnormalities, we performed a pathological analysis of TEKCRIF1 mice. To this end, we assessed the expression of MBP, an essential component in the myelination process, because damage to myelin sheaths and reductions in MBP result in defects in motor function in CNS diseases.^{26,27} MBP fluorescence intensity was reduced by approximately 40% in the cortex and by 60% in striatum of TEKCRIF1 mice compared with that in WT mice (Figure 2(a) and (b)) and the number of oligodendrocytes involved in the formation of myelin, Olig2⁺ cells were decreased by 25% in the cortex and striatum of TEKCRIF1 mice compared with that in WT mice without neuronal cell deaths except less than 5% developmental programmed cell deaths²⁸ in both WT and TEKCRIF1 mice, as assessed by TUNEL assay (Supplementary Figure 2 (a) to (d)). Furthermore, we examined the structure of myelin by electron microscopy and observed defects in myelin in TEKCRIF1 mice (Figure 2(c)). Whereas the myelin of WT mice was well organized, obvious swelling, decompression of the myelin sheath and loose myelin were observed in TEKCRIF1 mice. Myelin damage is indicative of BBB disruption and demyelination of CNS disorder.²⁹

In a normal state, the BBB maintains the immune privileged state of the brain by modulating the entry of immune cells into the CNS tissue.³⁰ Leukocyte infiltration is observed in CNS diseases such as multiple sclerosis with demyelination.^{27,31,32} To verify the infiltration of leukocytes in brain tissue, we performed immunohistochemistry with the anti-CD45 antibody in the cortex and striatum. CD45-positive cells considerably infiltrated the cortex and striatum of TEKCRIF1 mice (Figure 2(d) and (e)). We also performed a FACS analysis on brain tissue to investigate leukocyte subsets. We found that CD3⁺CD4⁺ T cells and CD3⁺CD8⁺ T cells increased in TEKCRIF1 mice compared with WT mice. Ly6C⁺ cells (monocytes) and Ly6G⁺ cells (neutrophils) were also increased in TEKCRIF1 mice compared with WT mice. These data suggest that the increase in CD45⁺ cells consisted of infiltrated T cells, neutrophils, and monocytes (Supplementary

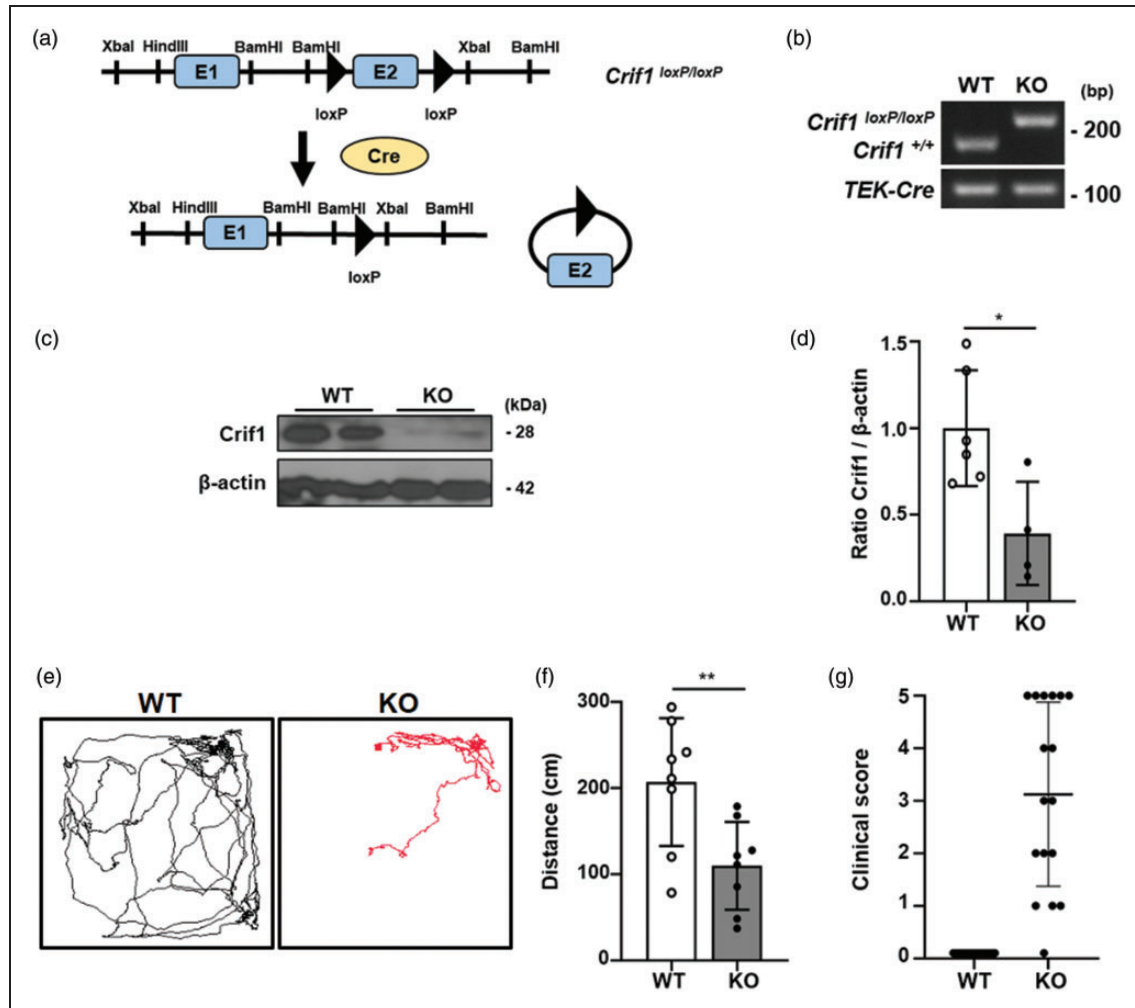


Figure 1. *Crif1* deletion in ECs induces behavioral abnormalities in TEKCRIF1 mice. (a) Schematic of the TEKCRIF1 gene locus. Exon 2 of *Crif1* was specifically knocked out in ECs by *TEK-Cre*. (b) Genotyping was performed by PCR using *Cre* and *Crif1* primers in WT: *TEK-Cre Crif1*^{+/+} mice and KO: *TEK-Cre Crif1*^{loxP/loxP} mice. (c, d) The *Crif1* protein level in the isolated microvessels from the brain tissue. (e, f) Movement activity of 11-day-old TEKCRIF1 mice was measured for 10 min in the open-field test (N = 8). (g) The behavioral defect was scored using a 5-point paradigm and plotted. Data are represented as the mean and SD; **P* < 0.05, ***P* < 0.01 compared with WT.

Table 1. Clinical score to determine the behavioral deficits in TEKCRIF1 mice.

Score	Description	Number of mice (WT)	Number of mice (KO)
0	No symptoms	17	
1	Floppy tail		4
2	Hindlimb weakness		3
3	Hindlimb paralysis		2
4	Forelimb and hindlimb paralysis		2
5	Death		6
	Total	17	17

The table shows the clinical score description (N = 17 per group).

Figure 2(e)). This infiltration means that *Crif1* deletion in ECs caused leukocyte infiltration in the CNS parenchyma. Taken together, these results suggest that endothelial-specific *Crif1* deletion causes behavior abnormalities through uncompacted myelin and leukocyte infiltration.

Crif1 deletion in ECs induces BBB disruption in TEKCRIF1 mice

To examine how myelin damage and leukocyte infiltration occur in TEKCRIF1 mice, we examined the expression of occludin as a tight junction molecule and albumin, and as a BBB leakage marker using

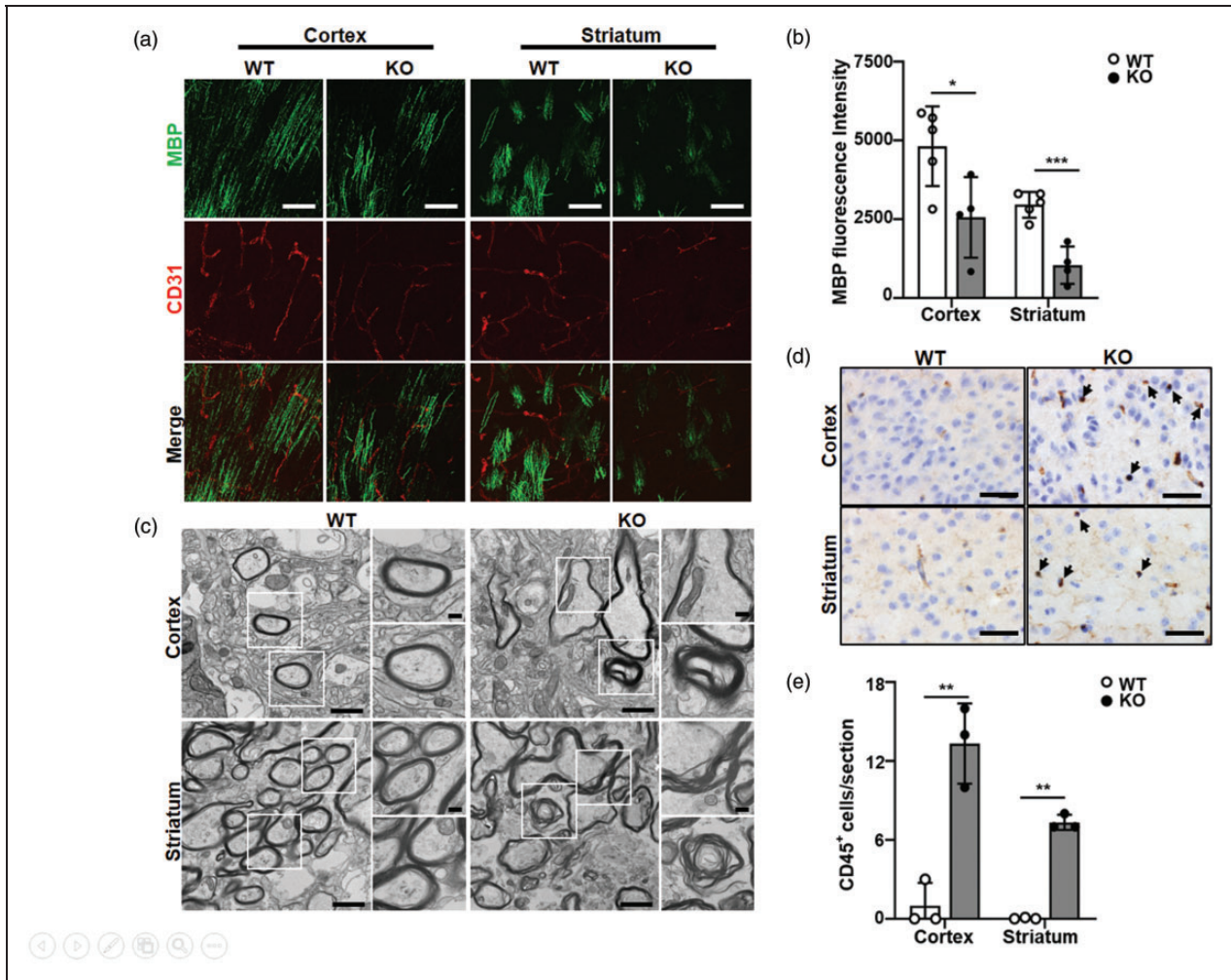


Figure 2. Uncompacted myelin and increase in leukocyte infiltration in TEKCRIF1 mice. (a) The cortex and striatum of TEKCRIF1 mice were stained for MBP (myelin basic protein; green) and CD31, a marker of ECs (red) (N = at least 4). Scale bar, 200 μ m. (b) The immunofluorescence staining intensity of MBP was quantified. Data are represented as the mean and SD; * $P < 0.05$, *** $P < 0.001$ compared with WT. (c) Electron microscopy images of myelin structure in the cortex and striatum of TEKCRIF1 mice (N = 3). Scale bar: 1 μ m, Rectangle: the enlarged images. Scale bar: 200 nm. (d, e) Infiltration of leukocytes (arrow) in the cortex and striatum of TEKCRIF1 mice stained for CD45 (N = 3). Scale bar: 60 μ m. Quantification of infiltrated CD45⁺ cells in the section. Data are represented as the mean and SD; ** $P < 0.01$ compared with WT.

immunofluorescence staining to determine whether the BBB is disturbed in TEKCRIF1 mice (Figure 3(a)). The fluorescence intensity of parenchymal albumin was increased to 1.5-fold in the cortex and 2-fold in the striatum in TEKCRIF1 mice compared with that in WT mice (Figure 3(c)). Triple-label immunofluorescence revealed that leakage of albumin was detected in regions where the expression of CD31, a marker of ECs, and occludin were decreased. Consistent with the immunostaining result, protein expression of occludin was decreased in the cortex and in the striatum compared with that in WT mice (Supplementary Figure 2(f) and (g)). We also examined claudin-5 protein which is one of the essential tight junction proteins for the

maintenance of BBB integrity in isolated microvessels from brain tissue. We found that claudin-5 protein expression in TEKCRIF1 mice was decreased by 70% of that in WT mice (Figure 3(e) and (f)).

To observe the BBB leakage in the mouse brain in a living state of mouse brain, in vivo dextran-FITC BBB permeability assay was performed using 40 kDa dextran, which is smaller than albumin (70 kDa). After dextran was injected into the heart of anesthetized TEKCRIF1 mice, the cortical vasculature was observed by two-photon imaging (Figure 3(g)).²¹ Imaging of the cortical vasculature clearly revealed that there was no leakage of dextran until 30 min after injection in WT mice. In contrast, significant

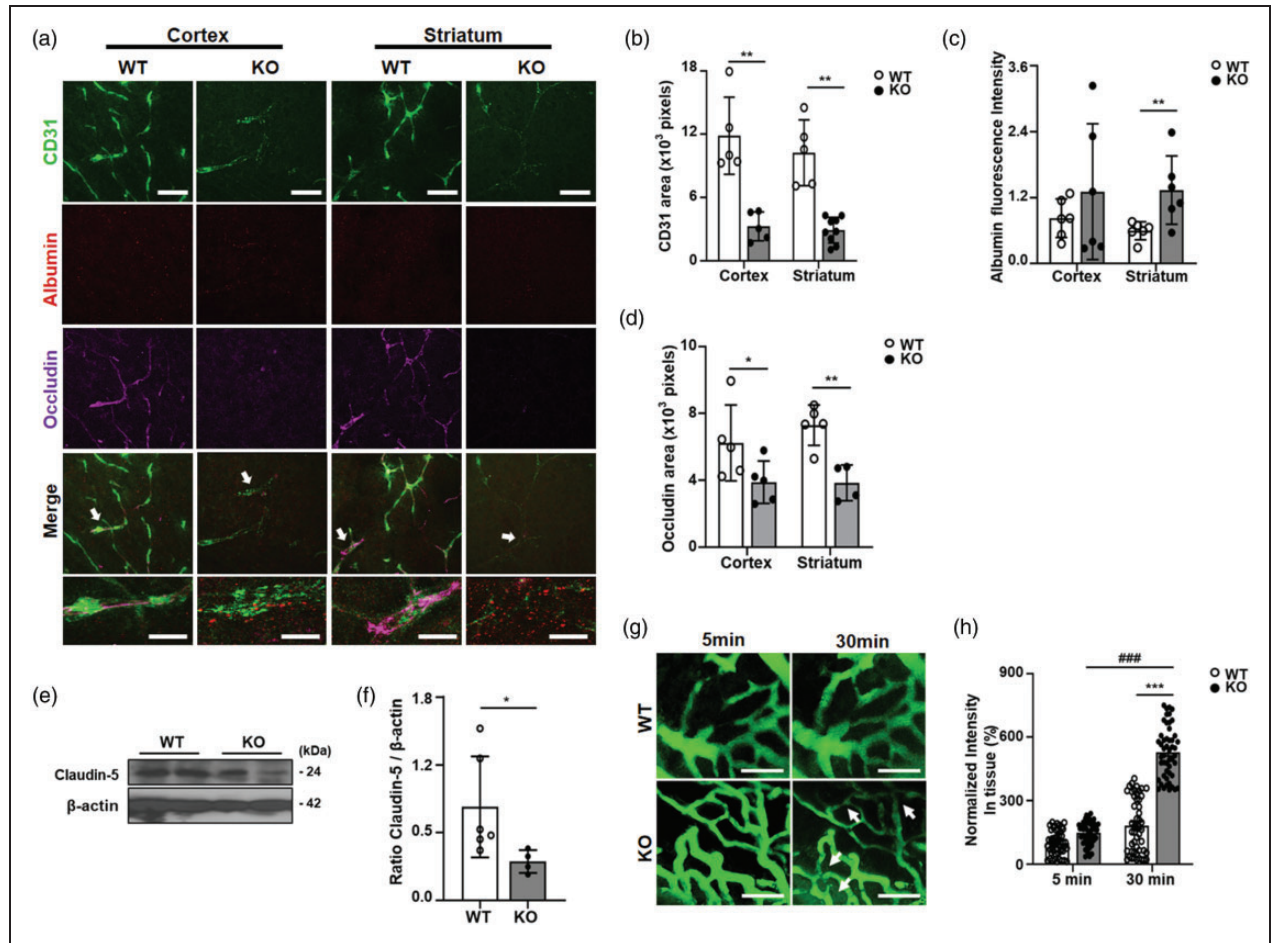


Figure 3. Endothelial-specific *Crifl* knockdown causes blood–brain barrier disruption in TEKCRIF1 mice. (a) Tissues were stained for CD31 (green), albumin (red), tight junction protein, and occludin (magenta) (N = at least 5). Scale bar: 20 μ m. Arrow indicated rectangle, enlarged region. Scale bar: 10 μ m. (b, c, d) The immunofluorescence staining area of CD31, occludin and area of albumin was quantified. Data are represented as the mean and SD; * $P < 0.05$, ** $P < 0.01$ compared with WT. (e) Protein levels of claudin-5 in the isolated microvessels from brain tissue of TEKCRIF1 mice were analyzed by Western blotting (N = at least 4). The intensity value of claudin-5 is shown in (f); * $P < 0.05$ compared with WT. (g) Leakage of dextran in TEKCRIF1 mice after injection of 40 kDa dextran-FITC. Arrows indicate leakage of dextran and the decrease in dextran in blood vessels. Scale bar: 50 μ m. (h) The dextran intensity was quantified with ROI boxes which indicate region of dextran leakage in tissue (n of ROI boxes = 50/group). Data are represented as the mean and SD; *** $P < 0.001$ compared with WT 30 min after dextran injection. #### $P < 0.001$ for the intensity compared between KO mice 5 min after dextran injection and 30 min after dextran injection.

dextran leakage over time was evident in TEKCRIF1 mice (Figure 3(g)). The vessels in WT mice were also more clearly detectable at 30 min than at 5 min owing to the circulating FITC-dextran in vessels. However, this decrease in dextran observed in vessels of the TEKCRIF1 mouse brain 30 min after injection indicates increased leakage into the tissue because of the escape of FITC-dextran from the vessels. FITC fluorescent vasculature images were quantitatively analyzed, and the intensity of the tissues near vessels was normalized (Figure 3(h)). While FITC intensity in the tissue did not differ between 5 min and 30 min after dextran injection in WT mice, FITC intensity in the tissue from TEKCRIF1 mice was obviously increased

30 min after dextran injection compared to the intensity 5 min after dextran injection. The real-time dextran leakage in the TEKCRIF1 mice brain strongly showed disrupted function of the BBB in vivo.

We examined whether *Crifl* deletion in ECs affects vessel formation by performing H&E staining on brain slices. We observed that the amount of normal blood vessels in TEKCRIF1 mice was decreased to 60% in the cortex and 50% in the striatum compared to that in WT mice (Supplementary Figure 3(a) and (b)). Then, we also examined whether vessel formation in the muscle was altered in TEKCRIF1 mice due to *Crifl* deletion and endothelial dysfunction. As shown in Supplementary Figure 3(c) and (d), there were no

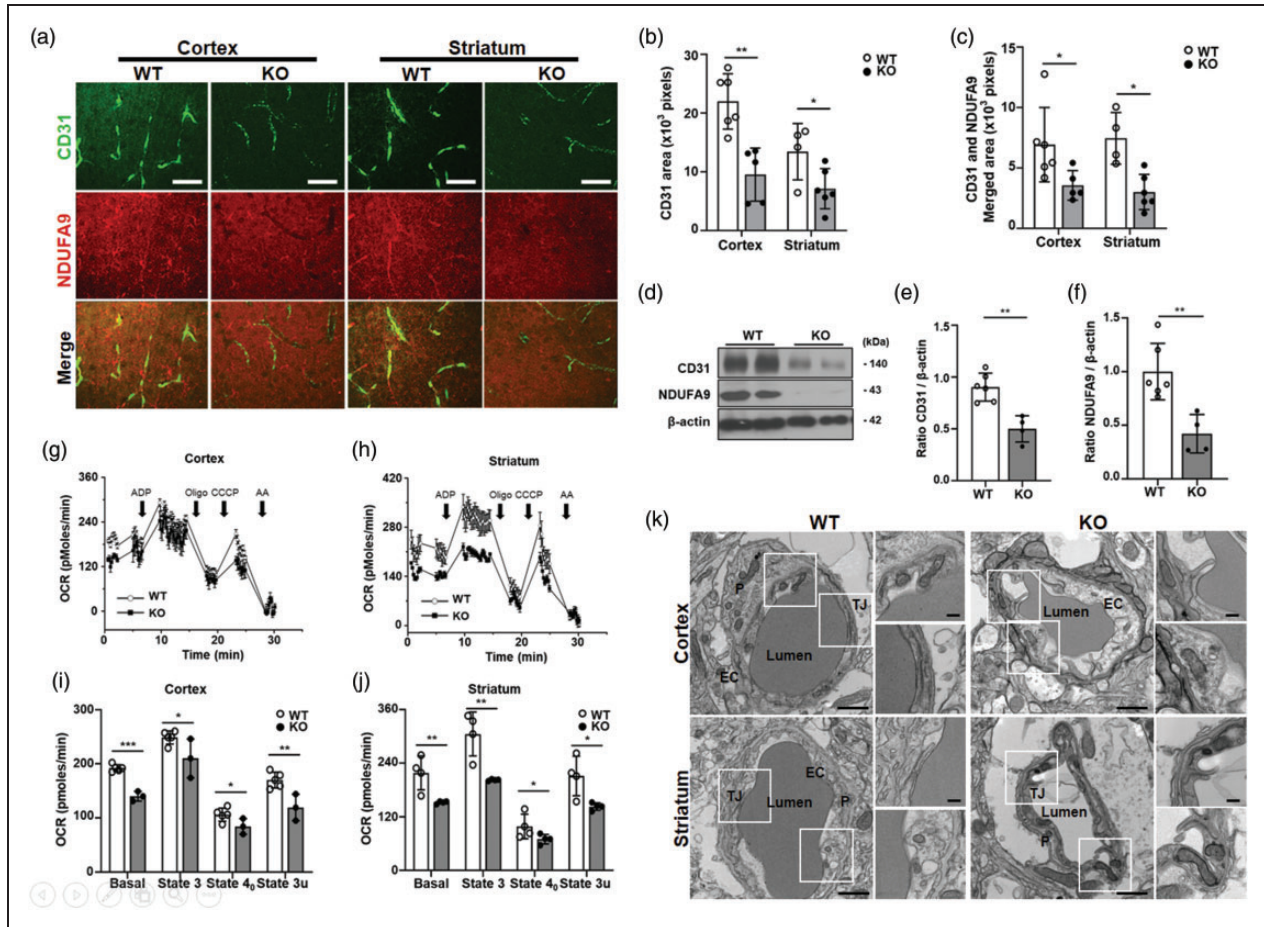


Figure 4. *Crif1* deletion leads to mitochondrial OXPHOS dysfunction in TEKCRIF1 mice. (a) The cortex and striatum were stained for CD31 (green) and NDUFA9, a maker of mitochondrial complex I (red) ($N =$ at least 4). Scale bar; 20 μm . (b, c) The immunofluorescence staining area of CD31 and merged area with CD31 and NDUFA9 was quantified. Data are represented as the mean and SD; * $P < 0.05$, ** $P < 0.01$, *** $P < 0.001$ compared with WT. (d) The CD31 and NDUFA9 protein expression in the isolated microvessels from brain tissue of TEKCRIF1 mice was analyzed by Western blotting ($N =$ at least 4). The intensity value of CD31 and NDUFA9 is shown in (e, f); * $P < 0.01$ compared with WT. (g, h) The oxygen consumption rate (OCR) in isolated mitochondria was analyzed by an XF24 analyzer to evaluate mitochondrial function in the cortex and striatum in TEKCRIF1 mice ($N =$ at least 3). Oligo: oligomycin, AA: antimycin A (i, j). Basal respiration and respiration in State 3 (ADP-stimulated respiration), State 4_o (oligomycin-stimulated respiration) and State 3_u (antimycin A-stimulated respiration) were quantified. (k) Electron microscopy images of the cerebrovascular structure in the cortex and striatum of TEKCRIF1 mice ($N = 3$). Scale bar: 1 μm , Rectangle: the enlarged images, Scale bar: 200 nm. EC: endothelial cell, TJ: tight junction, P: pericyte.

differences in blood vessel formation in the muscle between WT and TEKCRIF1 mice, and muscle morphology was well organized in TEKCRIF1 mice, similar to that in the WT mice. Occludin expression in the skeletal muscle is lower than in the brain for barrier formation.^{33,34} For this reason, we focused on ECs in the BBB. Since *Crif1* deletion in ECs decreased the number of blood vessels in brain, we performed tube-formation assays and investigated the levels of the angiogenesis-related genes, *Angpt2* and *Vegf*, using the bEnd.3 cell line to verify whether deletion of *Crif1* in ECs causes brain angiogenesis and vascular maturation (Supplementary Figure 3(e)). We observed

that siRNA-mediated knockdown of *Crif1* in bEnd.3 cells inhibited tube formation by 40% compared with control cells. These results are consistent with the reduction in vessel number found in the brains of TEKCRIF mice. However, *Vegf* mRNA expression was increased ~ 8 -fold in *Crif1*-knockdown bEnd.3 cells compared with control cells, whereas *Angpt2* expression was not significantly changed. These results indicate that *Crif1* deletion affects brain vascular barrier maturation and causes BBB disruption through inducing abnormalities in cerebral vascular morphology and downregulation of tight junction proteins at an early embryonic phase in TEKCRIF1 mice.

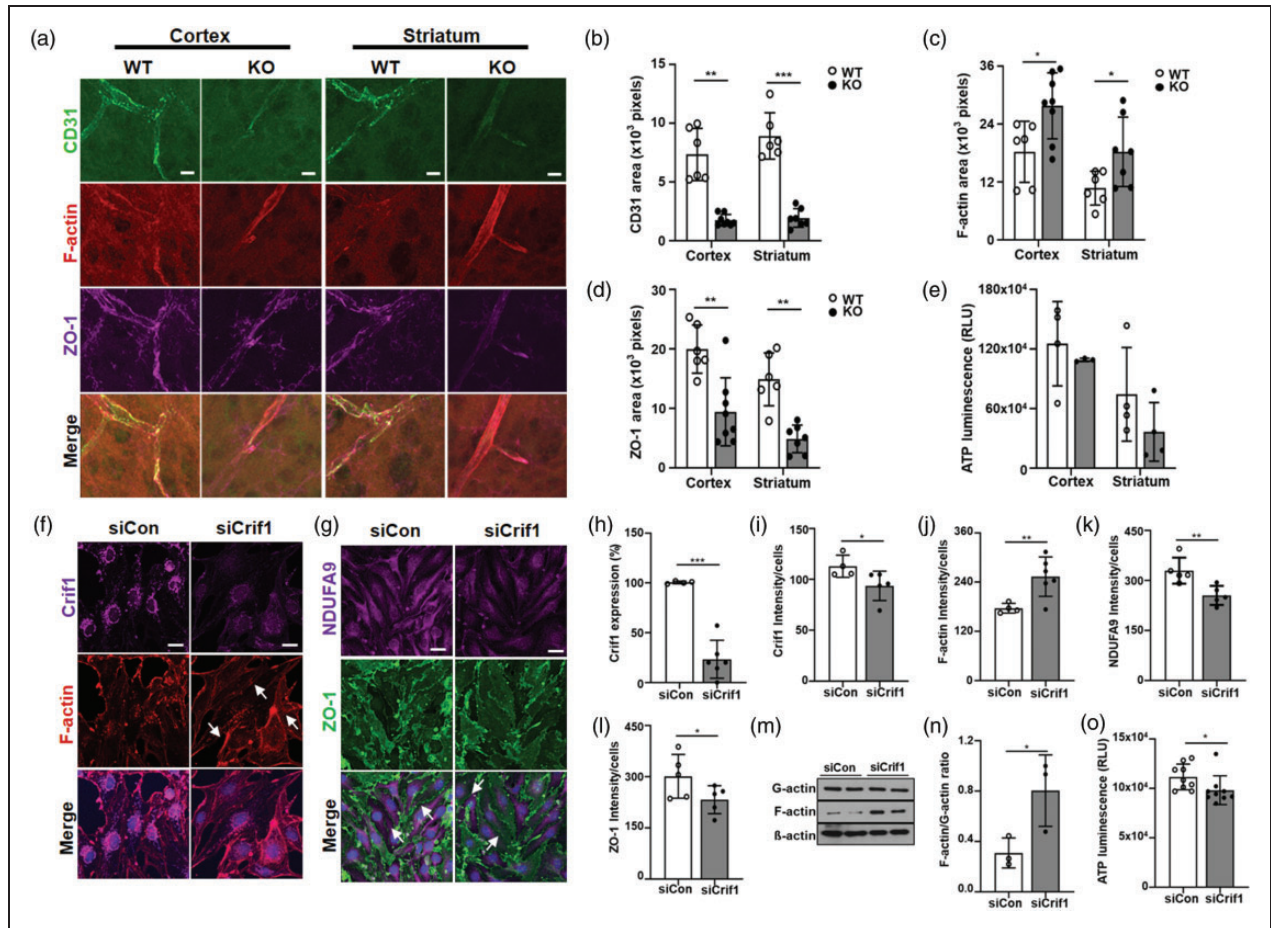


Figure 5. *Crifl* deletion induces alterations in actin cytoskeleton and junctional protein expression. (a) The cortex and striatum were stained for CD31 (green), F-actin (red) and ZO-1 (magenta), which is a tight junction-associated protein (N = at least 4, number of slides = at least 10). Scale bar: 10 μ m. (b–d) The fluorescent area of CD31, F-actin and ZO-1 was quantified in blood vessels. Data are represented as the mean and SD; * $P < 0.05$, ** $P < 0.01$, *** $P < 0.001$ compared with WT. (e) ATP bioluminescence assay was analyzed to determine the quantitative ATP content in the cortex and striatum of TEKCRIF1 mice (N = 4). (f) *Crifl* knockdown bEnd.3. cells and control cells were stained for Crifl (magenta) and F-actin (red) ($n =$ at least 4); Scale bar: 20 μ m. Arrows indicate an increase in F-actin expression. (g) *Crifl* knockdown bEnd.3. cells and control cells were stained for NDUFA9 (magenta) and ZO-1, a tight junction-associated protein (green) ($n =$ at least 4); Scale bar: 20 μ m. Arrows indicate a decrease in ZO-1 expression of siCrif1 compared to siCon. (h) Total percentage of *Crifl* expression was quantified. (i, j) Crif1 and F-actin intensity was quantified per cell. (k, l) The fluorescent intensity of NDUFA9 and ZO-1 was quantified per cell. Data are represented as the mean and SD; * $P < 0.05$, ** $P < 0.01$, *** $P < 0.001$ compared with control. (m) The expression of soluble G-actin, polymerized F-actin and total β -actin was examined by Western blotting ($n = 3$). (n) The ratio of F-actin to G-actin in bEnd.3. cells was quantified to observe an alteration in actin cytoskeleton. (o) ATP bioluminescence assay was analyzed to quantify the ATP content in bEnd.3. cells ($n = 9$). * $P < 0.05$ compared with control.

Crifl deletion in ECs deteriorates the blood vessels accompanying mitochondrial dysfunction

Because we found that the BBB was disrupted in TEKCRIF1 mice, we identified how the *Crifl* deletion in ECs led to BBB disruption through vascular defects. Double immunofluorescence staining in the cortex and striatum using the EC marker, CD31, and mitochondrial complex I marker, NDUFA9, was performed. As shown in Figure 4(a), TEKCRIF1 mice showed the decreased area of CD31 staining compared with WT mice (Figure 4(b)) as well as a decrease in the area of

CD31 and NDUFA9 co-staining (Figure 4(c)). These results suggest that EC-specific *Crifl* knockout leads to mitochondrial defects and cerebral vascular dysfunction. Consistent with these results, CD31 and NDUFA9 protein levels were decreased in microvessels isolated from the brains of TEKCRIF1 mice compared to those of WT mice (Figure 4(d) to (f)).

We also analyzed the OCR of isolated mitochondria from the cortex and striatum of TEKCRIF1 mice to verify the influence on metabolism induced by *Crifl* deletion. Both the basal OCR and the OCR of State 3, which is the state after ADP injection, of

isolated mitochondria from the cortex and striatum were reduced in TEKCRIF1 mice compared to those in WT mice (Figure 4(g) and (h)). Despite ADP supply, the OCR in TEKCRIF1 mice was lower than that in WT mice, indicating that ATP production may be broken down in TEKCRIF1 mice, consistent with the ATP analysis. The OCR of State 4₀ (after oligomycin injection) and State 3_u (after CCCP injection) was also decreased by *Crif1* deletion (Figure 4(i) and (j)). To specify whether *Crif1* deletion-induced mitochondrial dysfunction in ECs impaired BBB integrity, we transfected bEnd.3 cells, a mouse cerebral cortex EC line, with small interfering RNA (siRNA) to decrease *Crif1* expression. *Crif1* knockdown in bEnd.3 cells resulted in decreased *Crif1* mRNA and Crif1 protein expression with decreased protein expression of the mitochondrial complex I subunit, NDUFA9 (Supplementary Figure 4 (a) and (b)). The oxygen consumption rate was also decreased in *Crif1* knockdown cells. Compared to negative siRNA-transfected cells (siCon), *Crif1* knockdown cells (siCrif1) showed reduced basal respiration before treatment with oligomycin (Oligo), an inhibitor of ATP synthase (Supplementary Figure 4(c) and (d)). The oxygen consumption rate after treatment with oligomycin revealed that there is less consumption in *Crif1* knockdown cells than in control cells, suggesting that ATP production is lower in *Crif1* knockdown cells than in control cells. After CCCP treatment, which causes an uncoupling of the proton gradient in the electron transport chain, *Crif1* knockdown cells showed less of an increase in the OCR than control cells, indicating that *Crif1* deletion resulted in a lower maximal respiration and spare capacity than in control cells.

According to Figure 4(k), which shows the cerebral vascular structure by electron microscopy, healthy mitochondria with distinct cristae were observed to overlap with ECs in WT mice by interacting via tight junctions. In TEKCRIF1 mice, however, damaged mitochondria were observed, including abnormal mitochondrial cristae and an unorganized interaction between cerebrovascular ECs. Furthermore, the overlapped region of ECs was shorter and broken. These results suggest that EC-specific *Crif1* deletion induced cerebral vascular damage and BBB disruption caused by mitochondrial dysfunction.

***Crif1* loss causes dysregulation of actin dynamics and a decrease in tight junction-associated protein expression via ATP depletion**

Thus far, we have demonstrated that *Crif1* deletion in ECs leads to abnormal behavior caused by myelin damage and leukocyte infiltration through cerebrovascular dysfunction and BBB disruption. Therefore, to investigate how BBB disruption occurs with *Crif1*

deletion-induced endothelial dysfunction, we focused on the role of ATP depletion in *Crif1* deletion-induced mitochondrial dysfunction based on the importance of ATP for maintaining the interaction between tight junctions and the actin cytoskeleton.¹² ATP depletion in cells causes an alteration in the F-actin/G-actin ratio through the dysregulation of actin dynamics. In the early phase of BBB disruption, an increase in the F-actin ratio induces alterations in tight junction and tight junction-associated proteins in ECs accompanying the BBB disruption.³⁵ We observed changes in F-actin and zonula occludens-1 (ZO-1) protein expression in the cortex and striatum of TEKCRIF1 mice. *Crif1* deficiency led to increased F-actin expressed area by 33% in the cortex and 45% in the striatum of TEKCRIF1 mice with a decrease in CD31 expressed area in ECs compared with that in WT mice (Figure 5(a) to (d)). To identify the effects on metabolism function induced by *Crif1* deletion in the cortex and striatum of TEKCRIF1 mice, we performed an ATP assay. Although there was no significant difference, there was a trend toward a reduction in ATP in TEKCRIF1 mice compared to that in WT mice (Figure 5(e)). We observed clear mitochondrial dysfunction in the isolated mitochondrial OCR analysis (Figure 4(e) and (f)) as with the ATP analysis.

We investigated the expression of F-actin and ZO-1, a tight junction-associated protein, in *Crif1* knockdown cells. Consistent with the change of F-actin and ZO-1 expression in vivo, the percentage of Crif1 expression was decreased by approximately 80% in *Crif1* knockdown cells, and Crif1 fluorescent intensity was reduced by 25% compared in each cell to that in control (Figure 5 (f), (h) and (i)), accompanied by an increase in the F-actin intensity to 135% in each cell compared to that in control (Figure 5(f) and (j)). Consistent with the decrease in NDUFA9 expression observed in the in vivo study, NDUFA9 expression also decreased by 25% in siCrif1 cells compared with that in control cells, and the ZO-1 fluorescent intensity was verified to be reduced by 25% in siCrif1 cells compared with that in control (Figure 5(g), (k), and (l)). To further verify the rearrangement of F-actin and G-actin, we analyzed the F-actin/G-actin ratio. The F/G-actin ratio was significantly increased in siCrif1 cells compared to that in siCon cells, with no significant change in total β -actin protein expression (Figure 5(m) and (n)). Consistent with the OCR analysis, the relative ATP concentration in siCrif1 cells was lower than that in siCon cells (Figure 5(o)). Taken together, these data indicate that mitochondrial dysfunction with ATP depletion through *Crif1* knockdown induced an alteration in actin cytoskeleton and tight junction-associated protein expression. These data show that *Crif1* deletion caused dysregulation of the actin cytoskeleton and ZO-1 expression accompanying the decrease in ATP production caused by

mitochondrial dysfunction in the cortex and striatum of TEKCRIF1 mice.

BBB disruption was observed in brain of VECad Cre-ER^{T2}-*Crif1*^{flox/flox} mice by stereotaxic injection of endoxifen

We investigated whether the *Crif1* deletion induced BBB disruption in the brain specifically in VECad (VE-cadherin, vascular endothelial cadherin promoter) Cre-ER^{T2}-*Crif1*^{flox/flox} mice. To delete *Crif1* in ECs of the brain, we crossed *Crif1*-floxed C57BL6/J mice with VECad Cre-ER^{T2} mice expressing a tamoxifen-inducible *Cre* recombinase under the control of the VE-cadherin promoter.³⁶ The mice were injected stereotaxically with endoxifen, a metabolite of tamoxifen, into the striatum.³⁷ Activated *Cre* expression was confirmed in brain tissue of endoxifen-injected VECad Cre-ER^{T2}-*Crif1*^{flox/flox} mice by PCR. The deleted-gene product resulting from activated *Cre* recombinase was identified in endoxifen-injected VECad Cre-ER^{T2}-*Crif1*^{flox/flox} mice, but not in control mice (Supplementary Figure 5(a) and (b)). To observe BBB disruption in endoxifen-injected VECad Cre-ER^{T2}-*Crif1*^{flox/flox} mice, we examined the expression of CD31 and the albumin and ZO-1 protein in the region where endoxifen was injected. Compared to that in the control group, CD31 expression was decreased in endoxifen-injected VECad Cre-ER^{T2}-*Crif1*^{flox/flox} mice (Figure 6(a), (b), (d), and (e)). Consistent with the results in TEKCRIF1 mice, albumin leakage showed BBB disruption accompanying the decrease of ZO-1, in the tight junction-associated protein (Figure 6(c) and (f)). However, owing to the short observation period, leukocyte infiltration was rare in acute endoxifen-injected VECad Cre-ER^{T2}-*Crif1*^{flox/flox} mice (Supplementary Figure 5(c)). These results demonstrated that *Crif1* deletion specifically in ECs in the brain can cause BBB disruption in not only TEKCRIF1 mice but also in endoxifen-injected VECad Cre-ER^{T2}-*Crif1*^{flox/flox} mice. As shown in Figure 6(g), an EC-specific *Crif1* deficiency resulted in BBB maturation and disruption. This disruption in the BBB in TEKCRIF1 mice leads to abnormal behaviors in association with immune cell infiltration and myelin damage accompanied by dysregulation of the actin cytoskeleton and junctional proteins. In addition, endoxifen-injected VECad Cre-ER^{T2}-*Crif1*^{flox/flox} mice, in which *Crif1* was deleted specifically in the striatum area, exhibited BBB disruption together with a leakage of albumin and reduction in tight junction-associated proteins.

Discussion

BBB disruption is considered to be a result of oxygen–glucose depletion in ischemic stroke and a symptom of neurodegenerative diseases such as Parkinson's disease and Alzheimer's disease.³⁸ Tight junction assembly in ECs is indispensable for the maintenance of BBB strength. However, therapeutics of BBB disruption has been targeting secondary injury and glial cells surrounding the BBB. A recent study showed that cyclooxygenase inhibition prevents BBB disruption following ischemic stroke.³⁹ Although oxidative stress causes BBB disruption and pathogens aggravate BBB dysfunction in neurological diseases, whether mitochondrial modulation in ECs can preserve BBB integrity is still unknown. In addition, BBB disruption has not been examined in an endothelial cell-specific mitochondria-targeted genetic animal model. Here, we reveal that endothelial-specific *Crif1* deletion induced BBB disruption accompanied by an alteration in junctional protein expression and the actin cytoskeleton caused by dysfunction of mitochondrial energy metabolism.

We observed loose and damaged myelin sheaths in TEKCRIF1 mice and showed leakage of the albumin and immune cells in TEKCRIF1 mice. The infiltration of the substances through the weak BBB leads to brain tissue damage. In addition, we investigated the increase of immune cells such as T cells, monocytes and neutrophils in the brain of TEKCRIF1 mice by FACS analysis. Leakage of a plasma protein promotes chemokine release and T cell recruitment and demyelination.⁴⁰ However, the analysis of slides prepared from endoxifen-injected VECad Cre-ER^{T2}-*Crif1*^{flox/flox} mice revealed that CD45⁺ cells were scarce owing to the short observation period. Increased BBB permeability was also observed early (within 1 h) after traumatic brain injury (TBI) and recovered after 6 h, whereas leukocyte adherence was detected more than 6 h after TBI and was independent of BBB damage.^{41,42} These reports, taken together with our experimental results, suggest that disruption of the BBB is not always accompanied by leukocyte infiltration. The severity of mitochondrial dysfunction may affect pathophysiological responses, such as leukocyte infiltration and inflammation. We demonstrate that the infiltration of immune cells through the broken BBB can induce myelin damage and behavioral deficits associated with neurological pathologies in TEKCRIF1 mice, but the direct relationship between the immune system and myelin damage needs to be investigated in further studies. In this study, we focused on mitochondrial function in ECs of the BBB, which provides the energy necessary to maintain the cytoskeleton and junctional proteins of the BBB.

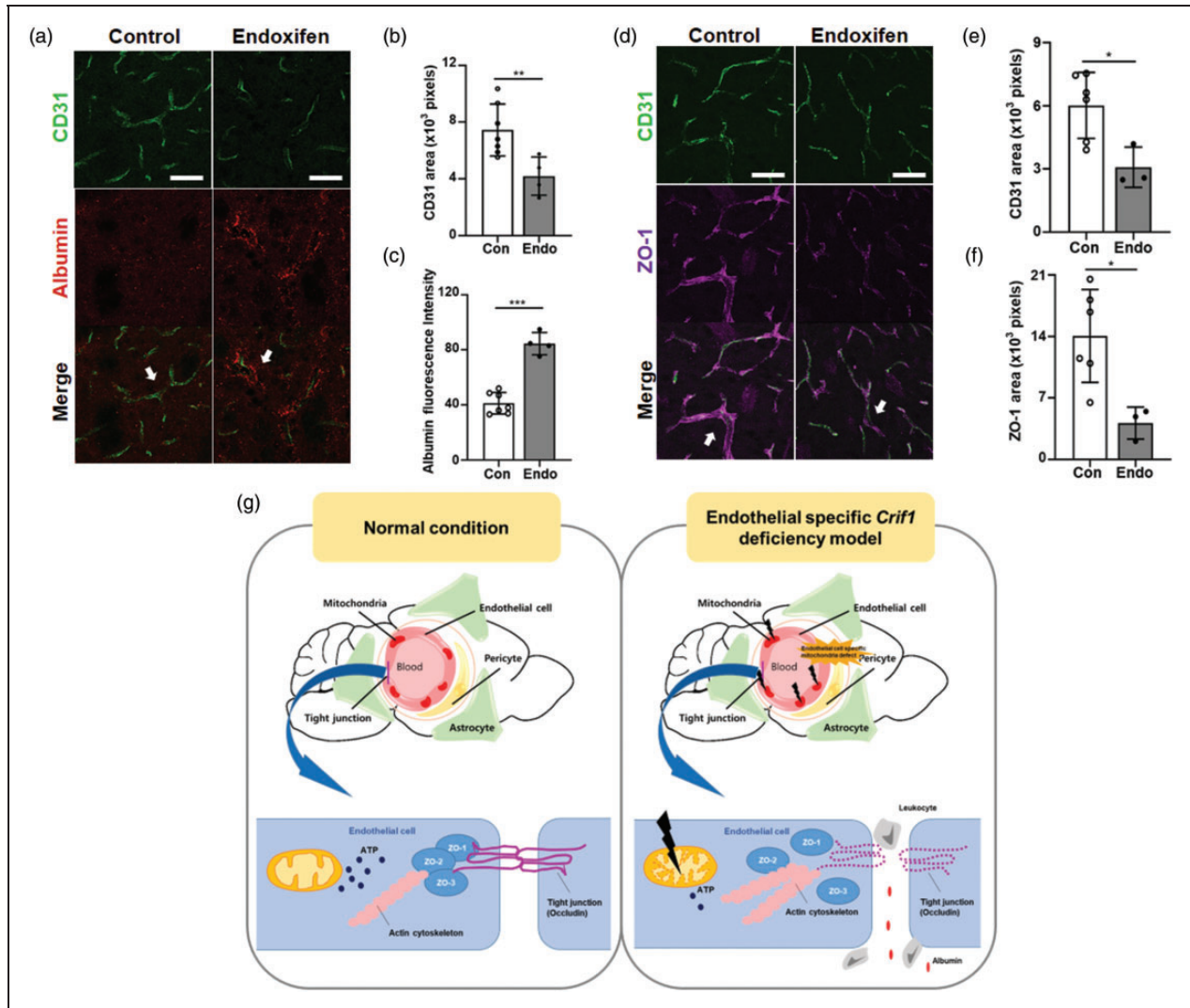


Figure 6. *Crif1* deletion in ECs generates BBB disruption in VECad Cre-ERT²-*Crif1*^{flox/flox} mice. (a) The striatum of VECad Cre-ERT²-*Crif1*^{flox/flox} mice, endoxifen injected were stained for CD31 (green), Albumin (red). Control is the group injected 20% DMSO/PBS, Endoxifen is the group injected 2.5 mM endoxifen hydrochloride hydrate in 20% DMSO/PBS (N = at least 4). Scale bar: 10 μ m. Arrows indicate an albumin leakage of endoxifen compared to control. (b, c) The fluorescent area of CD31 and intensity of albumin was quantified. Data are represented as the mean and SD; * $P < 0.05$, ** $P < 0.01$, *** $P < 0.001$ compared with control. (d) The striatum of VECad Cre-ERT²-*Crif1*^{flox/flox} mice, endoxifen injected were stained for CD31 (green), ZO-1 (magenta). Scale bar: 10 μ m. Arrows indicate a decrease in ZO-1 expression of endoxifen compared to control (N = at least 3). (e, f) The fluorescent area of CD31 and ZO-1 was quantified. Data are represented as the mean and SD; * $P < 0.05$ compared with control. (g) Schematic of the mechanism underlying mitochondrial dysfunction in ECs of the BBB. *Crif1* deletion in ECs causes mitochondrial dysfunction in the ECs of the BBB. ATP depletion resulted from mitochondrial dysfunction affects actin dynamics and increases F-actin in ECs. These changes lead to dysregulation of the interaction between the actin cytoskeleton and junctional proteins that maintain BBB integrity. Plasma proteins and peripheral immune cells cross the broken BBB. Infiltrated substances cause secondary injury such as myelin damage, inducing behavioral deficits.

Crif1 is a prime target in the investigation of mitochondrial OxPhos function as a protein that is crucial in the formation of the mitochondrial OxPhos polypeptides in the mitochondrial membrane.¹⁸ We identified the reduction of NDUFA9 (mitochondrial complex I subunit) protein expression with isolated microvessels from the brain of TEKCRIF1 mice. Furthermore, we showed that *Crif1* deficiency impaired junctional

proteins that maintain BBB integrity with isolated microvessels from brain through the ATP depletion by analyzing the mitochondrial oxidative consumption rate in cerebral ECs. In pathological conditions such as ischemic stroke, the actin cytoskeleton is reorganized by actin depolymerizing factor (ADF)/cofilin signaling.³⁵ In addition, RhoA/ROCK signaling is related to regulating BBB permeability by inducing stress

fibers and increasing EC contractility.⁴³ Even though several molecules modulate the actin cytoskeleton, we suggest the importance of ATP from mitochondria in ECs for BBB integrity because cerebral ECs are different from peripheral ECs, which have fewer mitochondria and use energy provided by glycolysis.⁴⁴ Meanwhile, in the neurovascular unit, the BBB consists of ECs, pericytes and astrocytes. Pericyte- and astrocyte-covered blood vessels regulate the BBB by secreting numerous factors.⁴⁵ In TEKCRIF1 mice, secreted molecules from pericytes and astrocytes and the related signaling need to be examined in future studies.

Additionally, a reduction in both glycolysis and mitochondrial oxidative phosphorylation affects angiogenesis and vascular barrier maturation in retina and brain vessels.⁴⁶ The increase in reactive oxygen species that accompanies deletion of Tmm7 (translocase of outer mitochondrial membrane 7) inhibits brain angiogenesis and formation of cerebrovascular network.⁴⁷ We found the defects of vessel formation in the brain of TEKCRIF1 mice, while there were no differences in blood vessel formation in the muscle between WT and TEKCRIF1 mice. Besides, *Crif1*-knockdown bEnd.3 cells showed decrease of tube formation compared to Control. However, *Crif1* defect in bEnd.3 cells showed no difference in *Angpt2* mRNA expression and increase of *Vegf* mRNA expression. We interpret these findings as indicating that mature vessel formation was inhibited owing to insufficient mitochondrial ATP support, while vascular EC expression of growth factors was upregulated by oxidative stress as part of a vascular homeostasis mechanism.^{15,48} These data suggest that a *Crif1* deficiency not only disrupts the BBB, but also results in defective vascular maturation owing to mitochondrial dysfunction in cerebrovascular ECs, not peripheral vessels. Collectively, it is clear that *Crif1* deletion altered BBB integrity in TEKCRIF1 mice with a genetic mitochondrial defect beginning in the embryonic phase as well as VECad Cre-ER^{T2}-*Crif1*^{flox/flox} mice with acute mitochondrial dysfunction induced by endoxifen injection in the adult phase, as confirmed by a decrease in tight junction protein expression and an increase in albumin leakage.

In summary, the present study shows that *Crif1* downregulation induced a decrease in ATP production in mitochondria OxPhos in ECs of the BBB. This change disrupted the interaction between the actin cytoskeleton, tight junction-associated proteins and tight junction proteins in the ECs of the BBB, which have more mitochondria than peripheral ECs. Moreover, *Crif1* downregulation caused abnormal behaviors by immune cell infiltration and myelin damage through impairing BBB integrity. Thus, we investigated the role of mitochondrial OxPhos in the

ATP supply in cerebral ECs. These data contribute to the understanding of the maintenance of BBB integrity from a position of ECs and mitochondria in ECs of the BBB, which may be a novel target to help attenuate the progression of BBB disruption in cerebrovascular diseases and neurodegenerative diseases.

Funding

The author(s) disclosed receipt of the following financial support for the research, authorship, and/or publication of this article: This work was funded by the National Research Foundation of Korea (NRF) grant, the Ministry of Science and ICT (MSIT) (2017R1A5A2015385), (2019R1F1A1059586), the Bio & Medical Technology Development Program (2019M3E5D1A02068575). This work was supported by IBS-R015-D1, IBS-R011-D1 and Global Research Laboratory (GRL) Program (2017K1A1A2013124).

Declaration of conflicting interests


The author(s) declared no potential conflicts of interest with respect to the research, authorship, and/or publication of this article.

Authors' contributions

MJL, YSJ, JYH and GRK made substantial contributions to the conception and design of the study. MJL and YSJ were responsible for the acquisition of data and provided materials for experiments. MJL and YSJ helped with the analysis and interpretation of data. MJL, YSJ, JYH and GRK wrote the manuscript. JSH, MJR, SJK, XJ, YLL, JC, JZ, SYC, WSC, CJH, HSY, HJK, YHH, SKC and MHS contributed to the discussion and revised the article and all approved the final version of the manuscript. JYH and GRK are responsible for the integrity of the work as a whole.

ORCID iDs

Jeongsu Han  <https://orcid.org/0000-0001-6524-9841>

Jun Y Heo  <https://orcid.org/0000-0002-0859-0063>

Supplemental material

Supplemental material for this article is available online.

References

1. Rellick SL, Hu H, Simpkins JW, et al. Evaluation of bioenergetic function in cerebral vascular endothelial cells. *J Visual Exp* 2016; 117: 54847.
2. Doll DN, Hu H, Sun J, et al. Mitochondrial crisis in cerebrovascular endothelial cells opens the blood-brain barrier. *Stroke* 2015; 46: 1681–1689.
3. Alluri H, Stagg HW, Wilson RL, et al. Reactive oxygen species-caspase-3 relationship in mediating blood-brain barrier endothelial cell hyperpermeability following oxygen-glucose deprivation and reoxygenation. *Microcirculation* 2014; 21: 187–195.

4. Bukeirat M, Sarkar SN, Hu H, et al. MiR-34a regulates blood-brain barrier permeability and mitochondrial function by targeting cytochrome c. *J Cereb Blood Flow Metab* 2016; 36: 387–392.
5. Oldendorf WH, Cornford ME and Brown WJ. The large apparent work capability of the blood-brain barrier: a study of the mitochondrial content of capillary endothelial cells in brain and other tissues of the rat. *Ann Neurol* 1977; 1: 409–417.
6. Kemper MF, Zhao Y, Duckles SP, et al. Endogenous ovarian hormones affect mitochondrial efficiency in cerebral endothelium via distinct regulation of PGC-1 isoforms. *J Cereb Blood Flow Metab* 2013; 33: 122–128.
7. Loscher W and Potschka H. Blood-brain barrier active efflux transporters: ATP-binding cassette gene family. *NeuroRx* 2005; 2: 86–98.
8. Tsukamoto T and Nigam SK. Tight junction proteins form large complexes and associate with the cytoskeleton in an ATP depletion model for reversible junction assembly. *J Biol Chem* 1997; 272: 16133–16139.
9. Wallez Y and Huber P. Endothelial adherens and tight junctions in vascular homeostasis, inflammation and angiogenesis. *Biochim Biophys Acta* 2008; 1778: 794–809.
10. Qin LH, Huang W, Mo XA, et al. LPS Induces occludin dysregulation in cerebral microvascular endothelial cells via MAPK signaling and augmenting MMP-2 levels. *Oxidat Med Cell Long* 2015; 2015: 120641.
11. Liu WY, Wang ZB, Zhang LC, et al. Tight junction in blood-brain barrier: an overview of structure, regulation, and regulator substances. *CNS Neurosci Thera* 2012; 18: 609–615.
12. Suurna MV, Ashworth SL, Hosford M, et al. Cofilin mediates ATP depletion-induced endothelial cell actin alterations. *Am J Physiol Renal Physiol* 2006; 290: F1398–1407.
13. Shen L and Turner JR. Actin depolymerization disrupts tight junctions via caveolae-mediated endocytosis. *Mol Biol Cell* 2005; 16: 3919–3936.
14. Kluge MA, Fetterman JL and Vita JA. Mitochondria and endothelial function. *Circ Res* 2013; 112: 1171–1188.
15. Caja S and Enríquez JA. Mitochondria in endothelial cells: sensors and integrators of environmental cues. *Redox Biol* 2017; 12: 821–827.
16. Ventura-Clapier R, Garnier A and Veksler V. Transcriptional control of mitochondrial biogenesis: the central role of PGC-1 α . *Cardiovasc Res* 2008; 79: 208–217.
17. Scarpulla RC. Nuclear control of respiratory chain expression by nuclear respiratory factors and PGC-1-related coactivator. *Ann N Y Acad Sci* 2008; 1147: 321–334.
18. Kim SJ, Kwon MC, Ryu MJ, et al. CRIF1 is essential for the synthesis and insertion of oxidative phosphorylation polypeptides in the mammalian mitochondrial membrane. *Cell Metab* 2012; 16: 274–283.
19. Nagar H, Jung S, Ryu MJ, et al. CR6-interacting factor 1 deficiency impairs vascular function by inhibiting the Sirt1-eNOS pathway. *Antioxid Redox Signal* 2017; 27: 234–249.
20. Okabe K, Kobayashi S, Yamada T, et al. Neurons limit angiogenesis by titrating VEGF in retina. *Cell* 2014; 159: 584–596.
21. Heo C, Park H, Kim Y-T, et al. A soft, transparent, freely accessible cranial window for chronic imaging and electrophysiology. *Sci Rep* 2016; 6: 27818.
22. Lee YK, Uchida H, Smith H, et al. The isolation and molecular characterization of cerebral microvessels. *Nat Protoc* 2019; 14: 3059–3081.
23. Banks WA, Gray AM, Erickson MA, et al. Lipopolysaccharide-induced blood-brain barrier disruption: roles of cyclooxygenase, oxidative stress, neuroinflammation, and elements of the neurovascular unit. *J Neuroinflamm* 2015; 12: 223.
24. Chow BW and Gu C. The molecular constituents of the blood-brain barrier. *Trends Neurosci* 2015; 38: 598–608.
25. Gurfein BT, Zhang Y, Lopez CB, et al. IL-11 regulates autoimmune demyelination. *J Immunol* 2009; 183: 4229–4240.
26. Homma S, Jin X, Wang G, et al. Demyelination, astrogliosis, and accumulation of ubiquitinated proteins, hallmarks of CNS disease in deficient mice. *J Neurosci* 2007; 27: 7974.
27. Ponsford M, Mazza G, Coad J, et al. Differential responses of CD45(+ve) T-cell subsets to MBP in multiple sclerosis. *Clin Exp Immunol* 2001; 124: 315–322.
28. White LD and Barone S, Jr. Qualitative and quantitative estimates of apoptosis from birth to senescence in the rat brain. *Cell Death Differ* 2001; 8: 345–356.
29. Miron VE, Kuhlmann T and Antel JP. Cells of the oligodendroglial lineage, myelination, and remyelination. *Biochim Biophys Acta* 2011; 1812: 184–193.
30. Graesser D, Solowiej A, Bruckner M, et al. Altered vascular permeability and early onset of experimental autoimmune encephalomyelitis in PECAM-1-deficient mice. *J Clin Invest* 2002; 109: 383–392.
31. Schmitt C, Strazielle N and Ghersi-Egea J-F. Brain leukocyte infiltration initiated by peripheral inflammation or experimental autoimmune encephalomyelitis occurs through pathways connected to the CSF-filled compartments of the forebrain and midbrain. *J Neuroinflamm* 2012; 9: 187–187.
32. Larochelle C, Alvarez JI and Prat A. How do immune cells overcome the blood-brain barrier in multiple sclerosis? *FEBS Letters* 2011; 585: 3770–3780.
33. Hwang I, An BS, Yang H, et al. Tissue-specific expression of occludin, zona occludens-1, and junction adhesion molecule A in the duodenum, ileum, colon, kidney, liver, lung, brain, and skeletal muscle of C57BL mice. *J Physiol Pharmacol* 2013; 64: 11–18.
34. Oldendorf WH and Brown WJ. Greater number of capillary endothelial cell mitochondria in brain than in muscle. *Proc Soc Exp Biol Med Soc Exp Biol Med* 1975; 149: 736–738.
35. Shi Y, Zhang L, Pu H, et al. Rapid endothelial cytoskeletal reorganization enables early blood-brain barrier disruption and long-term ischaemic reperfusion brain injury. *Nat Commun* 2016; 7: 10523.
36. Monvoisin A, Alva JA, Hofmann JJ, et al. VE-cadherin-CreERT2 transgenic mouse: a model for inducible recombination in the endothelium. *Dev Dyn* 2006; 235: 3413–3422.

37. Benedykcinska A, Ferreira A, Lau J, et al. Generation of brain tumours in mice by Cre-mediated recombination of neural progenitors in situ with the tamoxifen metabolite endoxifen. *Dis Models Mech* 2016; 9: 211–220.
38. Obermeier B, Daneman R and Ransohoff RM. Development, maintenance and disruption of the blood-brain barrier. *Nat Med* 2013; 19: 1584–1596.
39. Candelario-Jalil E, Taheri S, Yang Y, et al. Cyclooxygenase inhibition limits blood-brain barrier disruption following intracerebral injection of tumor necrosis factor- α in the rat. *J Pharmacol Exp Ther* 2007; 323: 488–498.
40. Ryu JK, Petersen MA, Murray SG, et al. Blood coagulation protein fibrinogen promotes autoimmunity and demyelination via chemokine release and antigen presentation. *Nature Commun* 2015; 6: 8164.
41. Hartl R, Medary M, Ruge M, et al. Blood-brain barrier breakdown occurs early after traumatic brain injury and is not related to white blood cell adherence. *Acta Neurochir Suppl* 1997; 70: 240–242.
42. Hartl R, Medary MB, Ruge M, et al. Early white blood cell dynamics after traumatic brain injury: effects on the cerebral microcirculation. *J Cereb Blood Flow Metab* 1997; 17: 1210–1220.
43. Gopalakrishnan S, Raman N, Atkinson SJ, et al. Rho GTPase signaling regulates tight junction assembly and protects tight junctions during ATP depletion. *Am J Physiol* 1998; 275: C798–809.
44. Tang X, Luo YX, Chen HZ, et al. Mitochondria, endothelial cell function, and vascular diseases. *Front Physiol* 2014; 5: 175.
45. Daneman R and Prat A. The blood-brain barrier. *Cold Spring Harbor Perspect Biol* 2015; 7: a020412.
46. Kim J, Kim YH, Kim J, et al. YAP/TAZ regulates sprouting angiogenesis and vascular barrier maturation. *J Clin Invest* 2017; 127: 3441–3461.
47. Shi D, Qi M, Zhou L, et al. Endothelial mitochondrial preprotein translocase Tomm7-Rac1 signaling axis dominates cerebrovascular network homeostasis. *Arterioscler Thromb Vasc Biol* 2018; 38: 2665–2677.
48. Kim YW and Byzova TV. Oxidative stress in angiogenesis and vascular disease. *Blood* 2014; 123: 625–631.